Journal of Applied Polymer Science

Styrene-butadiene-styrene copolymer compatibilized interfacial modified multiwalled carbon nanotubes with mechanical and piezoresistive properties

Lun Wang, Zhe Wang, Yue Wang, Xue Wang, Hengwei Wang, Guoming Lu, Dongyu Zhao, Zewen Li
Key Laboratory of Chemical Engineering Process and Technology for High-Efficiency Conversion, College of Heilongjiang Province, School of Chemistry and Materials Science, Heilongjiang University, Harbin 150080, People's Republic of China
Correspondence to: Z. Wang (E-mail: zhe.wang@msn.com)

ABSTRACT: In this study, styrene-butadiene-styrene tri-block copolymer/multiwalled carbon nanotubes (SBS/MWNTs) were prepared by means of a solution blending method. To enhance the compatibility between SBS and MWNTs, the SBS grafted MWNTs (SBS-*g*-MWNTs) were used to replace MWNTs. The MWNTs were chemically hydroxylated by the dissolved KOH solution with ethanol as solvent and then reacted with 3-Aminopropyltriethoxysilane (APTES) to functionalize them with amino groups (MWNT-NH_2). The SBS-*g*-MWNTs were finally obtained by the reaction of MWNT-NH_2 and maleic anhydride grafted SBS (MAH-*g*-SBS). The SBS-*g*-MWNTs were characterized by X-ray photoelectron spectroscopy (XPS), Fourier transform-infrared spectroscopy (FT-IR), transmission electron microscopy (TEM), scanning electron microscope (SEM), and thermogravimetric analysis (TGA). The results showed that the SBS molecules were homogeneously bonded onto the surface of the MWNTs, leading to an improvement of the mechanical and electrical properties of SBS/SBS-*g*-MWNTs composites due to the excellent interfacial adhesion and dispersion of SBS-*g*-MWNTs in SBS. A series of continuous tests were carried out to explore the electrical-mechanical properties of the SBS/SBS-*g*-MWNTs composites. We found out that, near the percolation threshold, the well-dispersed SBS/SBS-*g*-MWNTs composites showed good piezoresistive characteristics and small mechanical destructions for the development of little deformation under vertical pressure. © 2015 Wiley Periodicals, Inc. J. Appl. Polym. Sci. **2016**, *133*, 42945.

KEYWORDS: conducting polymers; copolymers; functionalization of polymers; grafting; mechanical properties

Received 25 May 2015; accepted 15 September 2015
DOI: 10.1002/app.42945

INTRODUCTION

As one of the most widely used thermoplastic elastomers, styrene-butadiene-styrene triblock copolymer (SBS) possesses advantages of both conventional rubbers and plastic polymers, originated from its unique microphase separation, has attracted much attention in recent years.[1–3] There have been many studies engaged to expand the application fields of SBS, such as getting SBS modified with different functional groups or incorporating various fillers into SBS matrix.[4,5] Among them it is practical to design carbon black as fillers to improve the mechanical property and impart it with some functionalities, such as electrical conductivity, thermal conductivity, and permeability resistance.[6–9] Nevertheless, too much carbon black impedes the microphase separation of SBS and strongly deteriorates the mechanical properties of the resulting composite.[10] Thus a new kind of fillers should be found to reduce the content of conductive filler required to achieve adequate conductivity, thus minimizes the influence on the microphase separation and the mechanical properties.

Carbon nanotubes (CNTs), which have displayed the combination of superlative mechanical, thermal, and electronic properties have caused great interests in science.[11–15] Due to the intrinsic superiority, the CNTs are promising fillers incorporated into SBS. However, the field that seeks to incorporate CNTs as polymer composite reinforcements has been beset by some crucial problems, such as the poor dispersion when mixed into the polymer matrix and the lack of interfacial bonding which limits load transfer from the polymer matrix to the nanotubes.[16–21] To overcome the disadvantages, an immense effort has been done such as high shear mixing, aid of surfactants, in situ polymerization and chemical functionalization.[22–27] For instance, Lu *et al.*[28] reported that SBS was reinforced with multiwalled carbon nanotubes (MWNTs) by the interaction through melt mixing. The tensile strength of SBS/MWNTs composites containing

© 2015 Wiley Periodicals, Inc.

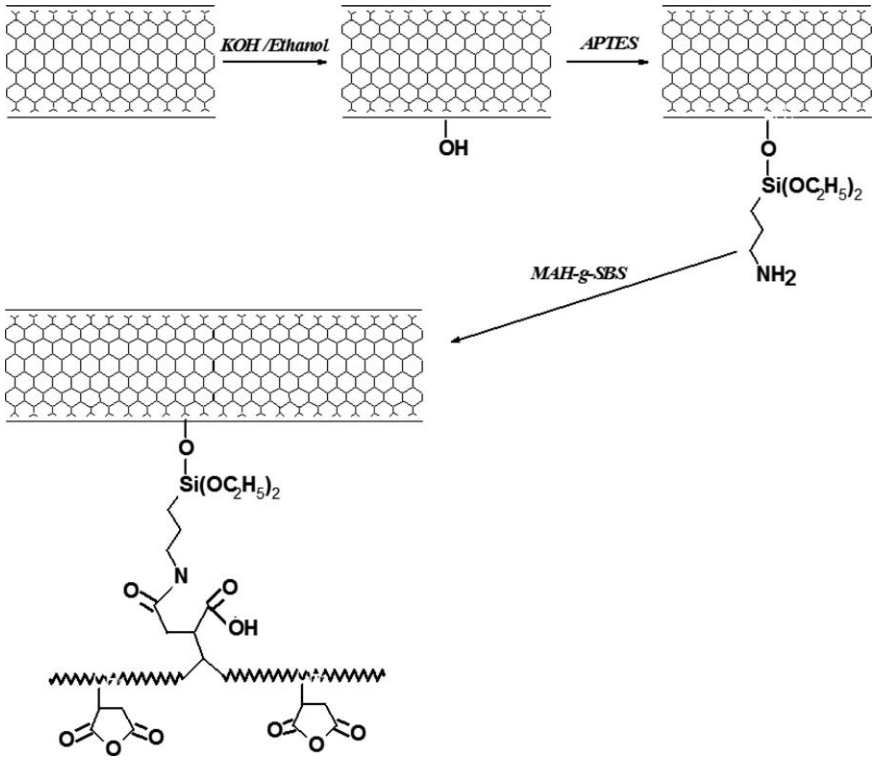

Figure 1. Schematic synthesis of route for SBS-*g*-MWNTs.

7 wt % MWNTs was 17.1 MPa, about 66% higher than that of pure SBS. However, the amount of functionalized MWNTs is small and there are still some MWNTs without any polymer coating, which leads to partially degradation of MWNTs in the matrix of SBS. To enhance the compatibility between SBS and MWNTs, the hydroxylated styrene-butadiene-styrene tri-block copolymer (HO-SBS) and the acyl chloride-activated MWNTs (MWNTs-COCl) were used to replace SBS and MWNTs, respectively which has been reported by Wu *et al.*[29] The highest tensile strength among nanocomposites, obtained from the sample of 4 wt % MWNTs, is 17.23 MPa. But in the process to prepare MWNT-COCl, the acid-treatments may largely destroy the structure of MWNTs, which would affect the properties of SBS/MWNTs composites. So that further studies about SBS/MWNTs composites should be conducted.

So far, no research was reported about the covalent grafting of SBS onto the surface of MWNTs, which could improve the dispersion of MWNTs in SBS matrix as well as increase their interfacial adhesion. In this study, SBS/SBS-grafted MWNTs composites with SBS containing maleic anhydride (MAH; MAH-*g*-SBS) and amine functionalized MWNTs were prepared. This study is devoted to prepare the nanocomposites from SBS and MWNTs by a solution processing method and to explore the mechanical, electrical and piezoresistive properties. The SBS-grafted MWNTs filled with SBS showed improved mechanical performance compared with the pure SBS and SBS reinforced with traditionally functionalized MWNTs. We believe that the improvement was due to the covalent bonding of polymer chains to MWNTs, where strong chemical bonds and a conjugated network between the nanotubes and polymers were established. Moreover, the SBS-grafted MWNTs had obvious effects on the SBS elevated electrical conductivity and it really perform good piezoresistive characteristics. It is a new way to synthesis SBS/SBS-grafted MWNTs composites with different MWNTs ratios and the conductive polymer composites.

EXPERIMENTAL

Materials

MWNTs (purity >95%, diameter 10 nm–20 nm) produced by chemical vapor deposition were obtained from Shenzhen Nanotech Port Co., Ltd. (China). MAH-*g*-SBS (2 wt % MAH) was prepared in this group. SBS (4402) was from Yanshan branch of China Petroleum Chemical Co. (3-Aminopropyl)-triethoxysilane (APTES) was purchased from the Chengdu Organic Chemistry Institute (China).

Synthesis of the Styrene-Butadiene-Styrene Copolymer-Grafted Multiwalled Carbon Nanotubes (SBS-*g*-MWNTs)

The scheme of synthesis route for the SBS-*g*-MWNTs, mainly through hydroxylation, amino functionalization and SBS modification of MWNTs, was showed in Figure 1. Previous studies about hydroxylation and amino functionalization of MWNTs were conducted in this work.[30,31] In a typical hydroxylation procedure, a large beaker was used as the container, 2.5 g of pristine MWNTs were added to the dissolved KOH solution with ethanol as solvent (40 g of KOH and 400 mL of ethanol). After ultrasonic dispersion for 30 min, the solution was refluxed for 12 h in a three-necked flask. The mixture was then respectively filtered by a membrane with a pore size of 0.2 μm, thoroughly washed with ethanol and deionized water three times and dried at 80°C under a vacuum for 12 h. The resulting product was

designated as MWNT-OH. The amino functionalization of MWNTs was carried out with an excess of APTES solution in mixed solution (2.0 g of MWNT-OH, 300 mL of DMF, 300 mL of toluene, and 30 mL of APTES). To ensure sufficient reaction, the mixture was stirred at 80°C for 10 h. Finally, the designated MWNT-NH_2 was obtained after washing with DMF and toluene, filtering, and drying procedures.

To synthesis SBS-*g*-MWNTs, before MAH-*g*-SBS and MWNT-NH_2 were blended in a mixer at a speed of 80 rpm at 110°C for 1 h with a weight ratio of 10:1 (15 g of MAH-*g*-SBS and 1.5 g of MWNT-NH_2), the MAH-*g*-SBS should be dissolved in 300 mL of toluene and the MWNT-NH_2 would be separately dispersed in toluene under ultrasonication to form a mixture. The temperature was turned down to 80°C and 30 mL of triethylamine was added as catalyst for another 36 h of reaction followed by washing with toluene, filtering, and drying.

Preparation of SBS/MWNTs and SBS/SBS-*g*-MWNTs Nanocomposites

SBS/MWCNTs composites were prepared by solution processing as following procedures. SBS was dissolved in the toluene with the ratio of 1:9 by weight to form a solution. MWCNTs were separately dispersed in toluene under ultrasonication to form a mixture. The SBS solution was poured into the mixture of MWCNTs/toluene. The mixture was under continuous stirring for 4 h. Meanwhile toluene was removed from the mixture. After all the toluene evaporated, resulting SBS/MWCNTs composites were obtained. The concentrations of MWCNTs in SBS are 1%, 3%, and 7.5% by weight. The SBS/SBS-*g*-MWNTs nanocomposites could be obtained as the same way above but to replace MWCNTs with SBS-*g*-MWNTs and the concentrations of MWCNTs in SBS were designed as 0.5 wt %, 1 wt %, 3 wt %, 5 wt %, 7.5 wt %, and 10 wt %. The composites were finally compression molded at 15 MPa and about 180°C for 10 min to form discs of 10 mm in diameter and 4.2 mm in thickness as well as dumbbell shape samples of 50 mm in length, 5.3 mm in width, and 3.2 mm in thickness. Two pieces of copper sheet were mounted onto the opposite wide surfaces of the discs sheets to ensure good electrical contact with DC current–voltage measurements for resistance (R) under piezoresistive tests at room temperature.

Measurements

X-ray photoelectron spectroscopy (XPS) was recorded on a Kratos-AXIS ULTRA DLD (Shimadzu Co., Japan) with an Al Kα X-ray source. Fourier-transform infrared (FT-IR) analysis was performed on a PerkinElmer Spectrum model 100 FT-IR spectrometer (Bruker Instruments Inc., Germany). Transmission electron microscopy (TEM) images of the nanocomposites were obtained with a JEM-2100 with 200 kV (Techcomp Ltd., Japan). Scanning electron microscope (SEM) images of the nanocomposites were obtained with a Hitachi S-4800 (Techcomp Ltd., Japan). Thermal gravimetric analyses (TGA) were conducted at 10°C/min from room temperature to 700°C under a nitrogen flow using a TGA 209 F1 analyzer (NETZSCH, Germany). Thermogravimetric and differential scanning calorimetry analyses (TG-DSC) were performed by a thermal analysis instrument (STA 449C, NETZSCH, Germany) from room temperature to 850°C at a temperature-ramping rate of 10°C/min in an air flow of 50 mL/min. The tensile strength and young's modulus of the composites were measured at room temperature with an R-9100 mechanical tester from Shen Zhen Rerer Instrument Co., Ltd., China. The strain rate was 5 mm/min with a load of 1 kN. The electrical resistivity was measured by a ZC36 megger from Shanghai No. 6 Electricity Meter Co., Ltd., China. The piezoresistive properties were measured using uniaxial dynamic pressure equipment in combination with DC current–voltage measurements (EST122 and HB-Z103-2AC source/measure units) from Shanghai No. 6 Electricity Meter Co., Ltd., China.

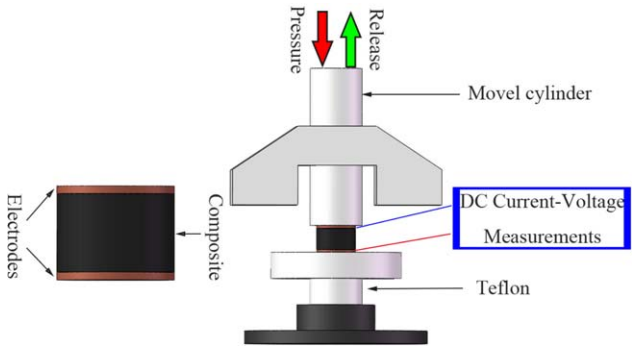

Figure 2. The experimental setup used to determine piezoresistive properties. [Color figure can be viewed in the online issue, which is available at wileyonlinelibrary.com.]

A special instrument (Figure 2) is introduced in this work to explore the electromechanical properties of SBS/SBS-*g*-MWNTs composites. At first, a vertical pressure is given to the composites and then get the pressure released, during which a dial indicator was used to measure the changed thickness of the samples (Δd). To avoid destroying the framework of the solid composites, the changes will be controlled under 5% thickness of the samples. Then the electrical resistance of SBS/SBS-*g*-MWNTs composites (R) was calculated from the slope of I–V curves measured, at room temperature, with EST122 picoammeter and HB-Z103-2AC high voltage DC power supply. At last, the electrical resistivity of the composites (ρ) during the pressure-release program was calculated by:

$$\rho = \frac{R \cdot A}{d - \Delta d}$$

where R is the electrical resistance of the samples, A is the area of the electrode, d is the thickness of the samples, and Δd is the changed thickness of the samples.

RESULTS AND DISCUSSION

Grafting of SBS onto the MWNTs

The FT-IR spectra of pristine MWNTs, MWNT-OH, MWNT-NH_2, and SBS-*g*-MWNTs was showed in Figure 3. For the pristine MWNTs showed in Figure 3(a), the appearance of a rather weak and broad absorption band at 3520 cm^{-1} was due to the presence of -OH groups on the surface of the pristine MWNTs; this resulted from either ambient atmospheric moisture bound to the MWNTs or oxidation during the purification of the raw MWNTs. The peak at 1630 cm^{-1} was ascribed to the stretching of the C=C groups in the structure of MWNTs. For the

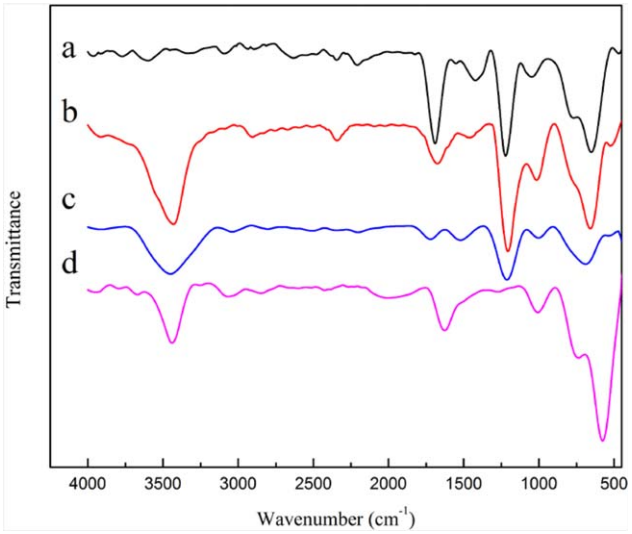

Figure 3. FT-IR spectra of (a) pristine MWNTs, (b) MWNT-OH, (c) MWNT-NH_2, (d) SBS-*g*-MWNTs. [Color figure can be viewed in the online issue, which is available at wileyonlinelibrary.com.]

MWNT-OH, in Figure 3(b), a strong and broad band at 3437 cm^{-1} was supposed to be the stretching vibration of the -OH group of the hydroxide functionality, and the peaks at 1026 cm^{-1} were attributed to the stretching of C—O. For the MWNT-NH_2 [Figure 3(c)], the slightly less intense band at 1580 cm^{-1} was assigned to the bending vibration of the N—H bond of the amide group. In addition, the signal of Si—O—Si bonds attributed to the attaching of APTES on MWNT-OH showed in the SBS-*g*-MWNTs was characterized by the stretching bands at 1020 cm^{-1}. What is more, the diminished peak at 3400 to 3520 cm^{-1}, indicated largely decreased -OH groups, could further prove the occurrence of the amino functionalization of MWNTs. The peaks at 625 cm^{-1} and 750 cm^{-1} [Figure 3(d)], regarded as the special absorption peaks of SBS, were attributed to the bending vibration of C—H in benzene and the bending vibration of C—H in butadiene, respectively. The previous changes found in the spectrum of SBS-*g*-MWNTs verified the SBS moieties grafted to the MWNTs through the amide bonds.

Table I. XPS Atomic Percentage Content

	Element (AT %)			
Samples	C	N	O	Si
MWNTs	97.19	NA	2.81	NA
MWNT-OH	95.81	NA	4.19	NA
MWNT-NH_2	93.51	1.37	4.54	0.58
SBS-*g*-MWNTs	96.43	0.41	2.99	0.17

XPS showed in Figure 4 was further carried out to obtain information about their surface composition and chemical bonding. Atomic percentages by XPS were listed in Table I. For the pristine MWNTs, aside from the main C—C peak at 285.1 eV, a weak O1s peak at 532.8 eV (O1s: 2.81 atom %) was attributed to atmospheric moisture or oxidation during the purification

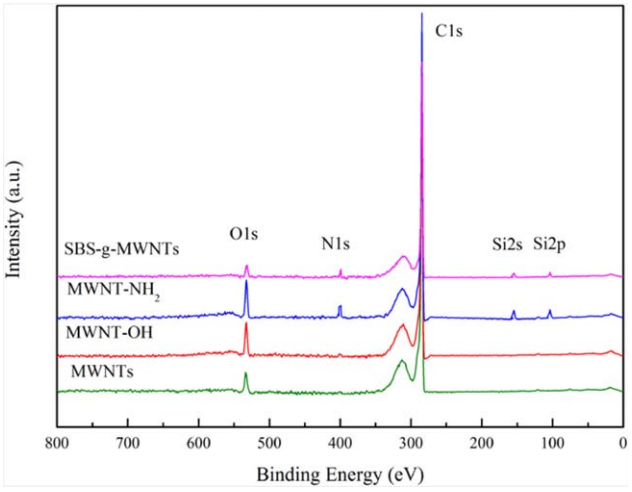

Figure 4. XPS full-scan spectra of pristine MWNTs, MWNT-NH_2, MWNT-OH, and SBS-*g*-MWNTs. [Color figure can be viewed in the online issue, which is available at wileyonlinelibrary.com.]

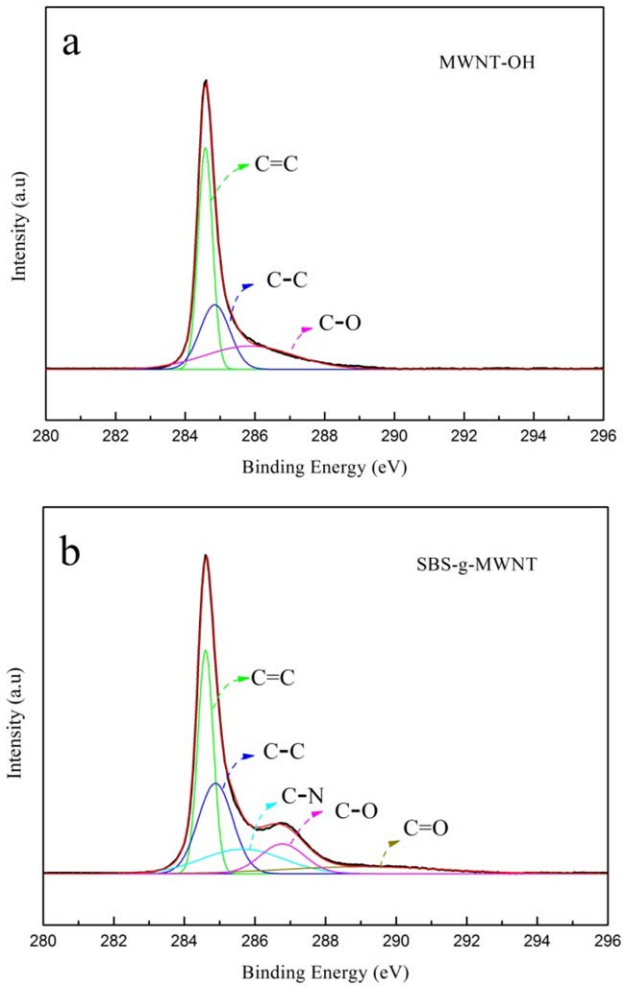

Figure 5. C1s XPS spectra of pristine MWNT-OH (a) and SBS-*g*-MWNTs (b). [Color figure can be viewed in the online issue, which is available at wileyonlinelibrary.com.]

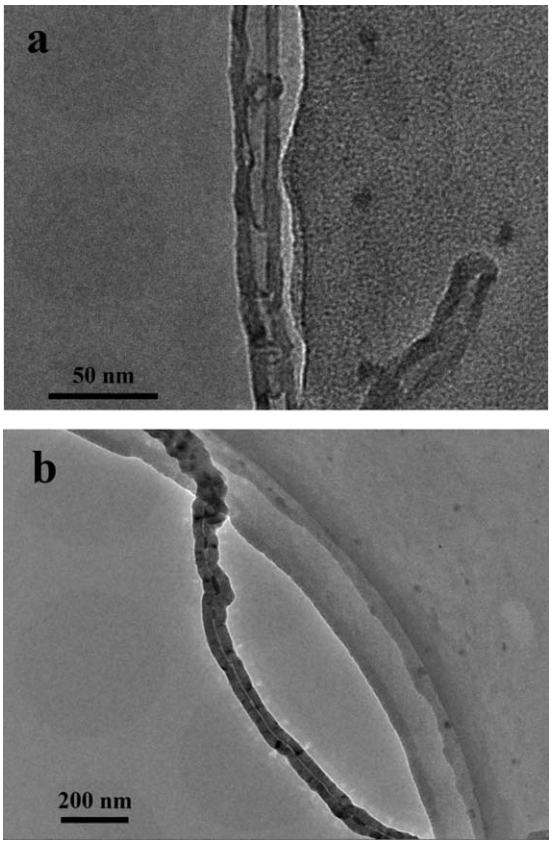

Figure 6. TEM micrographs of the (a) MWNT-OH and (b) SBS-*g*-MWNTs.

process. The percentage of oxygen increased up to 4.19 atom % in the process of hydroxylation. Two new photoemission peaks at 153.0 eV (Si2p: 0.58 atom %) and 400.0 eV (N1s: 1.37 atom %) appeared in the XPS spectrum of the MWNT-NH_2. Furthermore, the increased oxygen content was due to the hydrolysis of APTES. In the spectrum of SBS-*g*-MWNTs, compared with MWNT-NH_2, the peaks of Si2s and Si2p were diminished and the contain of carbon have obviously increased indicated that SBS have been attached to the surface of MWNT-NH_2. The carbon component C1s of MWNT-OH could be decomposed into three contributions appearing at 284.5 eV, 284.8 eV and 286.3 eV [Figure 5(a)]. The C1s peaks observed at 284.5 eV and 284.9 eV were, respectively interpreted as the combination of the sp^2 and sp^3 structure of MWNTs,[32] and the oxidized carbon peak emerges at 286.3 eV was contributed to the C in C—O bonds (hydroxyl group). In the spectrum of SBS-*g*-MWNTs [Figure 5(b)], it is interesting to notice that the binding energy of C=C (284.6 eV), C—C (284.9 eV), and C—O (286.7 eV) is higher than the corresponding binding energy of MWNT-OH. This is probably because of the coating of MAH-*g*-SBS changed the chemical environment of carbon, leading to the increase of binding energy. There are two new carbon peaks observed in the spectrum of SBS-*g*-MWNTs: the C in C—N bonds (amide groups, 285.9 eV) and the C in C=O bonds (anhydride groups, aldehyde groups, and amide groups, 289.3 eV).

Figure 6 showed the TEM images of MWNT-OH and the SBS-*g*-MWNTs after three times of washing with toluene under sonication to remove the unbound SBS completely. In the TEM image of MWNT-OH [Figure 6(a)], the MWNTs wall was relatively smooth, which means the structure of MWNTs have not been largely damaged by hydroxylation procedure. In contrast, the SBS-*g*-MWNTs showed in Figure 5(b) appeared stained with an extra phase presumed to mainly come from the grafted SBS molecules. We can also observe that the diameter of MWNT-OH is about 13 nm to 18 nm, whereas SBS-*g*-MWNTs (about 60–100 nm) are much thicker due to the wrapping of polymer. SEM images of MWNT-OH and SBS-*g*-MWNTs were shown in Figure 7. On the whole, the SEM observations were consistent with those from TEM, like the surface of MWNT-OH being relatively smooth, while for SBS-*g*-MWNTs, some salient parts appeared. The average diameter of SBS-*g*-MWNTs calculated from the scale mark is about 100 nm, which is roughly five times larger than MWNT-OH, in good agreement with the TEM observations.

One of the most important purposes to get CNTs functionalized is to improve the solubility or dispersion in organic solvents. In this work, a stable dispersion was obtained in the case of the SBS-*g*-MWNTs when equal amounts of MWNTs were added to the same volume of toluene, the good solvent of SBS, and mechanically mixed (Figure 8). As showed in Figure 8(a), all of nanotubes sank in the case of neat MWNTs. The explore about

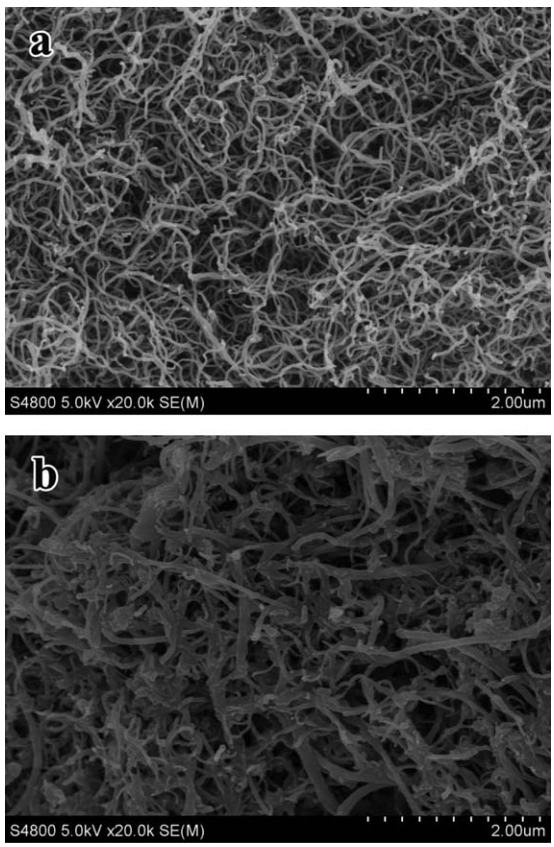

Figure 7. SEM micrographs of the (a) MWNT-OH and (b) SBS-*g*-MWNTs.

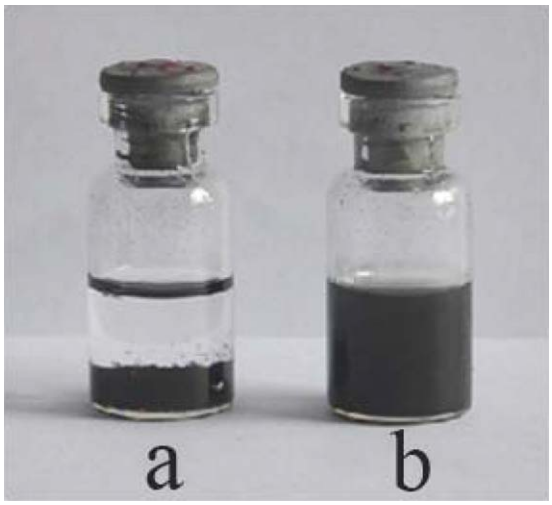

Figure 8. Photograph of (a) MWNTs and (b) SBS-*g*-MWNTs dispersed in chloroform and waited for 1 week. [Color figure can be viewed in the online issue, which is available at wileyonlinelibrary.com.]

the dispersion of SBS-*g*-MWNTs in SBS under the solution processing method was showed in Figure 9. SBS was dissolved in the toluene with the ratio of 1:9 by weight to form a SBS/toluene solution [Figure 9(a)]. Equal amounts of MWNTs [Figure 9(b)] and SBS-*g*-MWNTs [Figure 9(c)] were separately dispersed in SBS/toluene solution under ultrasonication and then kept at rest for 1 week. SBS-*g*-MWNTs showed much better dispersibility than MWNTs in SBS/toluene solution. This indicates that SBS-*g*-MWNTs possess a higher degree of miscibility than MWNTs due to the presence of SBS functional groups on the surface, as already proved above. Similar behavior has been observed in the case of polymer functionalized CNTs.[33]

The amount of the SBS grafted to the MWNTs was determined through the TGA analysis under a nitrogen atmosphere. Figure 10 show the mass loss variation of pristine MWNTs, SBS-*g*-

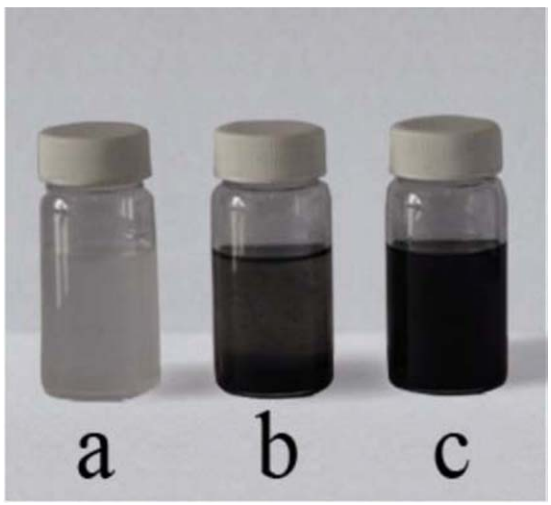

Figure 9. Photograph of (a) SBS/toluene solution; MWNTs (b) and SBS-*g*-MWNTs (c) dispersed in SBS/toluene solution and waited for 1 week. [Color figure can be viewed in the online issue, which is available at wileyonlinelibrary.com.]

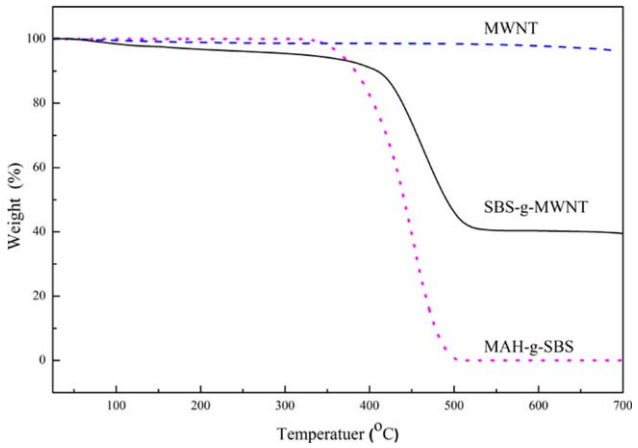

Figure 10. TGA traces of MAH-*g*-SBS, SBS-*g*-MWNTs, and MWNTs. [Color figure can be viewed in the online issue, which is available at wileyonlinelibrary.com.]

MWNTs, and MAH-*g*-SBS with increasing temperature. The MWNTs exhibit little weight loss during the program due to its conjugated structure, and when the temperature rise to 351°C the weight of MAH-*g*-SBS started to decrease and the weight percentage of SBS drop to as low as about zero at the temperature of 550°C. So that the weight loss of about 63 wt % during 351 to 550°C can be considered as the degradation of the grafted MAH-*g*-SBS on the MWNTs. The thermal stability of the materials was examined by thermal analysis (TG-DSC) in an air flow at a heating rate of 10°C/min (Figure 11). In the TG curve, the 63% weight loss of SBS-*g*-MWNTs during 302–395°C assigned to the ignition of MAH-*g*-SBS in an air flow fit the amount of MAH-*g*-SBS determined through the TGA analysis under a nitrogen atmosphere. The weight loss of MWNTs in SBS-*g*-MWNTs was during 562–707°C. And the ignition residues above 707°C are chiefly silicon oxide, which are introduced in the amino functionalization process. Based on the DSC curves, the exothermal peak of SBS-*g*-MWNTs around 352°C was higher than the exothermal peaks of pure MAH-*g*-SBS

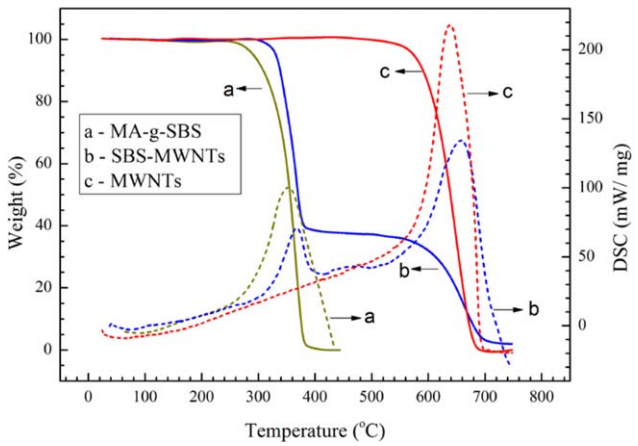

Figure 11. TG-DSC curves of (a) MAH-*g*-SBS, (b) SBS-*g*-MWNTs, and (c) MWNTs. [Color figure can be viewed in the online issue, which is available at wileyonlinelibrary.com.]

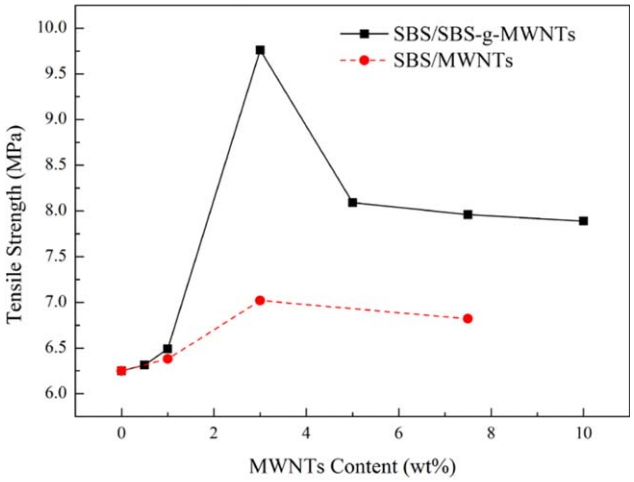

Figure 12. (a) Tensile strength and (b) Young's modulus curves of SBS/MWNTs and SBS/SBS-*g*-MWNTs composites. [Color figure can be viewed in the online issue, which is available at wileyonlinelibrary.com.]

(348°C), which means the thermal stability of the MAH-*g*-SBS was improved after it was grafted onto MWNTs.

Mechanical and Electrical Properties of SBS/SBS-*g*-MWNTs Composites

Figure 12 illustrates the tensile strength and young's modulus of SBS/MWNTs as well as SBS/SBS-*g*-MWNTs composites with various loadings of MWNTs. It was observed in Figure 12(a) that the tensile strength of the SBS/SBS-*g*-MWNTs composites with 3 wt % MWNTs loadings was 9.76 MPa increased by maxima of 56.16% compared with pure SBS (6.25 MPa). In Figure 12(b), the young's modulus of SBS/SBS-*g*-MWNTs composites with 0.5 wt % MWNTs loadings reached to 5.33 MPa increased by 61.52% compared with pure SBS (3.30 MPa). The further adding of SBS-*g*-MWNTs would contribute to higher young's modulus of SBS/SBS-*g*-MWNTs composites. For instance, the young's modulus of SBS/SBS-*g*-MWNTs composites with 3 wt % (8.21 MPa) and 10 wt % (17.51 MPa) MWNTs loadings increased by 148.78% and 430.61%, respectively compared with pure SBS. However, SBS/MWNTs composites have poorer mechanical properties than SBS/SBS-*g*-MWNTs composites. The tensile strength of the SBS/SBS-*g*-MWNTs composites is 2.75 MPa higher than SBS/MWNTs composites at a given MWCNT content of 3 wt %. The young's modulus of SBS/SBS-*g*-MWNTs composites with 7.5 wt % MWNTs loadings is 4.81 MPa higher than SBS/MWNTs composites with the same MWNTs loadings. There are two reasons for this difference in tensile strength. One reason is that the mechanical properties of the SBS/SBS-*g*-MWNTs composite were improved by the covalent chemical bonding of the polymer chains to the MWNTs. Another reason is that the stronger interfacial adhesion developed a better dispersion system and the mechanical properties of the SBS/SBS-*g*-MWNTs were improved in return.

The electrical resistivity of SBS/SBS-*g*-MWNTs composites with different MWNTs ratios were showed in Figure 13. As can be seen, the electrical resistivity of SBS/SBS-*g*-MWNTs composites decreases with increasing MWNTs loading. A sudden decrease in the resistivity, which is considered the percolation phenomenon, was observed as the mass fraction of MWNTs varies from 1 wt % to 3 wt %, indicating the formation of a preliminary conductive network. This low percolation concentration is consistent with those reported in previous work.[34] When the content of MWNTs reaches 7.5 wt %, the electrical resistivity of the composite has attained a value of 3.01×10^3 Ω m. Thereafter, the electrical resistivity stays on the same orders of magnitude with the further addition of MWNTs. In particular, the functionalization of MWNTs with SBS moieties is expected to improve the chemical affinity, the dispersion and their interactions with SBS, modifying therefore in a strong way the electrical conductivity.

Electromechanical Response under Vertical Compression

Electro-mechanical response of SBS/SBS-*g*-MWNTs composites with different loadings of MWNTs under vertical compression-rebound process were showed in Figure 14. Pure SBS considered as electrical insulator had no obvious piezoresistive property.

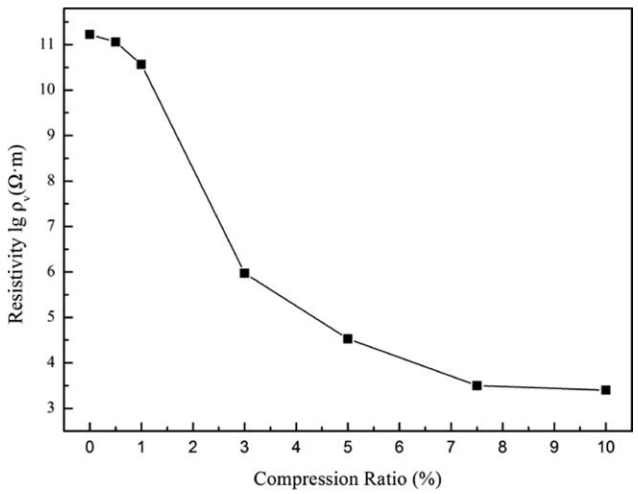

Figure 13. Electrical resistivity of pure SBS and the SBS/SBS-*g*-MWNTs composites with 0.5 wt %, 1 wt %, 3 wt %, 5 wt %, and 7.5 wt % loadings of MWNTs.

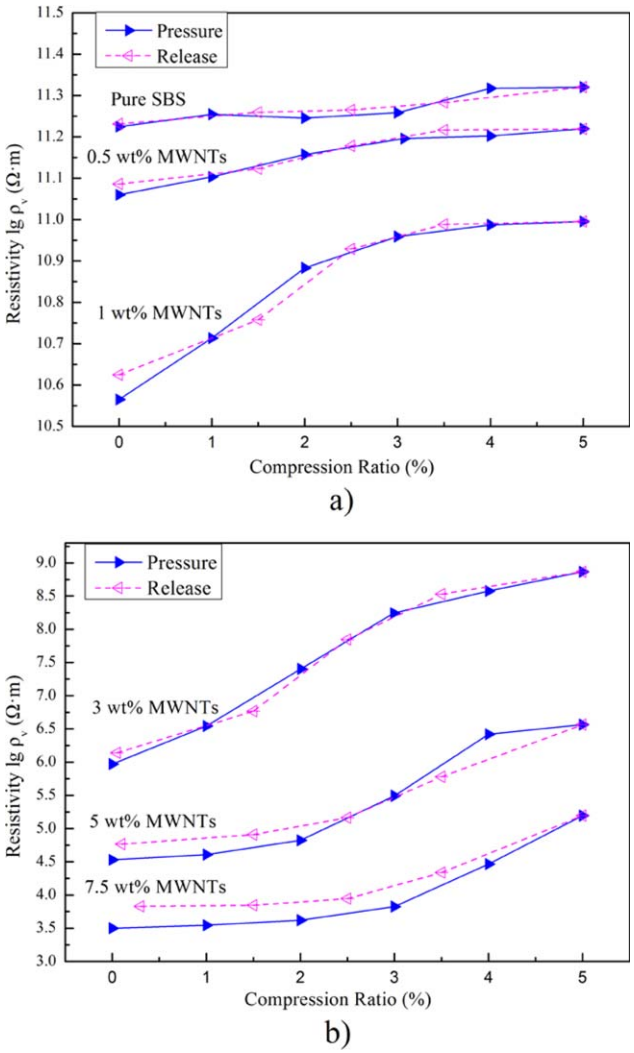

Figure 14. Electrical resistivity response under vertical compression-rebound of (a) pure SBS and the composites with 0.5 wt %, 1 wt %, (b) 3 wt %, 5 wt %, and 7.5 wt % loadings of MWNTs. [Color figure can be viewed in the online issue, which is available at wileyonlinelibrary.com.]

Below the percolation threshold, the composites with 0.5 wt % and 1 wt % of MWNTs showed little increase of electrical resistivity under vertical compression and when the pressure was released the electrical resistivity of the composites changed to almost the same value of its previous state. As long as the MWNTs content reached 3 wt %, near electrical percolation threshold, just small deformations could strong decrease the local concentration of the filler, which destroyed the conductive path between fillers and an obvious increase of the electrical resistivity occurred. But the further addition of MWNTs, would decrease the vibration of electrical resistivity during compression-rebound process. What's more, the electrical resistivity of 5 wt % and 7.5 wt % MWNTs content of the composites had little piezoresistive property when the compression ratio was below 2% thickness of the samples, and the electrical resistivity changed a lot by contrast with their preliminary after the pressure is released. This may be caused by the framework of the solid composites was damaged and the thickness of the samples would not recover to its original value even the pressure was completed released.

Taking above into account, the present work on piezoresistivity of SBS/SBS-*g*-MWNTs composites prepared with different contents of MWNTs in order to optimize the piezoresistive response. The best piezoresistive properties of SBS/SBS-*g*-MWNTs composites is near electrical percolation threshold, due to its sensitive to pressure as well as good mechanical recovery.

CONCLUSIONS

MWNTs were uniformly dispersed in the SBS matrix and developed excellent interfacial adhesion because of the novel structure of the SBS-*g*-MWNTs, as characterized by XPS, FT-IR, TGA, and TEM. The amount of the SBS grafted to MWNTs reached as high as 63 wt %. The tensile strength, young's modulus and electrical conductivity were all improved upon the addition of the SBS-*g*-MWNTs. The SBS-*g*-MWNTs filled with SBS were further studied for sensor applications due to its improved mechanical properties as well as excellent electrical performance and found out that SBS/SBS-*g*-MWNTs composites have excellent properties for piezoresistivity sensors under vertical compression near the percolation threshold.

ACKNOWLEDGMENTS

This study was supported by a grant from the National Natural Science Foundation of China (contract grant number 31270608) and the Heilongjiang Educational Committee (contract grant number 1511385).

REFERENCES

1. Airey, G. D. *Fuel* **2003**, *82*, 1709.
2. Ouyang, C.; Wang, S.; Zhang, Y.; Zhang., Y. *Polym. Degrad. Stab.* **2005**, *87*, 309.
3. Adhikari, R.; Michler, G. H. *Prog. Polym. Sci.* **2004**, *29*, 949.
4. Fu, B. X.; Lee, A.; Haddad, T. S. *Macromolecules* **2004**, *37*, 5211.
5. Li, H.; Wu, S.; Wu, J.; Huang, G. J. *Polym. Res.* **2014**, *21*, 1.
6. Al-Saleh, M. H.; Sundararaj, U. *Carbon* **2009**, *47*, 1738.
7. Inukai, S.; Niihara, K. I.; Noguchi, T.; Ueki, H.; Magario, A.; Yamada, E.; Endo, M. J. *Ind. Eng. Chem.* **2011**, *50*, 8016.
8. Fan, Z.; Luo, G.; Zhang, Z.; Zhou, L.; Wei, F. *Mater. Sci. Eng. B: Adv.* **2006**, *132*, 85.
9. Song, Y.; Xu, C.; Zheng, Q. *Soft Matter* **2014**, *10*, 2685.
10. Leyva, M. E.; Barra, G. M.; Moreira, A. C.; Soares, B. G.; Khastgir, D. *J. Polym. Sci. Part B: Polym. Phys.* **2003**, *41*, 2983.
11. Baughman, R. H.; Zakhidov, A. A.; de Heer, W. A. *Science* **2002**, *297*, 787.
12. Byrne, M. T.; Gun'ko, Y. K. *Adv. Mater.* **2010**, *22*, 1672.
13. Spitalsky, Z.; Tasis, D.; Papagelis, K.; Galiotis, C. *Prog. Polym. Sci.* **2010**, *35*, 357.
14. Oliva-Avilés, A. I.; Avilés, F.; Sosa, V. *Carbon* **2011**, *49*, 2989.

15. Lorenz, H.; Fritzsche, J.; Das, A.; Stöckelhuber, K. W.; Jurk, R.; Heinrich, G.; Klüppel, M. *Compos. Sci. Technol.* **2009**, *69*, 2135.
16. Chen, Y.; Liu, X.; Mao, X.; Zhuang, Q.; Xie, Z.; Han, Z. *Nanoscale* **2014**, *6*, 6440.
17. Frogley, M. D.; Ravich, D.; Wagner, H. D. *Compos. Sci. Technol.* **2003**, *63*, 1647.
18. Velasco-Santos, C.; Martínez-Hernández, A. L.; Fisher, F. T.; Ruoff, R.; Castano, V. M. *Chem. Mater.* **2003**, *15*, 4470.
19. Safadi, B.; Andrews, R.; Grulke, E. A. J. *Appl. Polym. Sci.* **2002**, *84*, 2660.
20. Guo, P.; Chen, X.; Gao, X.; Song, H.; Shen, H. *Compos. Sci. Technol.* **2007**, *67*, 3331.
21. Coleman, J. N.; Khan, U.; Blau, W. J.; Gun'ko, Y. K. *Carbon* **2006**, *44*, 1624.
22. Baibarac, M.; Baltog, I.; Lefrant, S.; Godon, C.; Mevellec, J. Y. *Chem. Phys. Lett.* **2005**, *406*, 222.
23. Ruan, S. L.; Gao, P.; Yang, X. G.; Yu, T. X. *Polymer* **2003**, *44*, 5643.
24. Peng, H.; Alemany, L. B.; Margrave, J. L.; Khabashesku, V. N. *J. Am. Chem. Soc.* **2003**, *125*, 15174.
25. Xu, J.; Zhang, A.; Zhou, T.; Cao, X.; Xie, Z. *Polym. Degrad. Stab.* **2007**, *92*, 1682.
26. Xu, H.; Li, B.; Wu, C. *Polym. J.* **2006**, *38*, 807.
27. Okpalugo, T. I. T.; Papakonstantinou, P.; Murphy, H.; McLaughlin, J.; Brown, N. M. D. *Carbon* **2005**, *43*, 153.
28. Lu, L.; Zhou, Z.; Zhang, Y.; Wang, S.; Zhang, Y. *Carbon* **2007**, *45*, 2621.
29. Wu, G.; Zhou, L.; Ou, E.; Xie, Y.; Xiong, Y.; Xu, W. *Mater. Sci. Eng. A* **2010**, *527*, 5280.
30. Song, P.; Shen, Y.; Du, B.; Guo, Z.; Fang, Z. *Nanoscale* **2009**, *1*, 118.
31. Liu, S.; Wang, Z.; Lu, G.; Wang, Y.; Zhang, Y.; He, X.; Zhao, D. *J. Appl. Polym. Sci.* **2014**, *131*.
32. Shulga, Y. M.; Tien, T. C.; Huang, C. C.; Lo, S. C.; Muradyan, V. E.; Polyakova, N. V.; Moravsky, A. P. *J. Electron Spectrosc.* **2007**, *160*, 22.
33. Gao, C.; Vo, C. D.; Jin, Y. Z.; Li, W.; Armes, S. P. *Macromolecules* **2005**, *38*, 8634.
34. Costa, P.; Ferreira, A.; Sencadas, V.; Viana, J. C.; Lanceros-Méndez, S. *Sens. Actuators A* **2013**, *201*, 458.